PHYSICAL REVIEW B **77**, 104514 (2008)

Limits to the critical current in $Bi_2Sr_2Ca_2Cu_3O_x$ tape conductors: The parallel path model

D. C. van der Laan
National Institute of Standards and Technology, Boulder, Colorado 80305, USA

J. Schwartz
National High Magnetic Field Laboratory, Florida State University, Tallahassee, Florida 32310, USA
and Department of Mechanical Engineering, FAMU-FSU College of Engineering, Tallahassee, Florida 32306, USA

B. ten Haken and M. Dhallé
Universiteit Twente, Enschede, The Netherlands

H. J. N. van Eck
FOM-Institute for Plasma Physics Rijnhuizen, Association EURATOM-FOM, Nieuwegein, The Netherlands
(Received 12 October 2007; revised manuscript received 21 December 2007; published 17 March 2008)

An extensive overview of a model that describes current flow and dissipation in high-quality $Bi_2Sr_2Ca_2Cu_3O_x$ superconducting tapes is provided. The parallel path model is based on a superconducting current running in two distinct parallel paths. One of the current paths is formed by grains that are connected at angles below 4°. Dissipation in this strongly linked backbone occurs within the grains and is well described by classical flux-creep theory. The other current path, the weakly linked network, is formed by superconducting grains that are connected at intermediate angles (4°–8°) where dissipation occurs at the grain boundaries. However, grain boundary dissipation in this weakly linked current path does not occur through Josephson weak links, but just as in the strongly linked backbone, is well described by classical flux creep. The results of several experiments on $Bi_2Sr_2Ca_2Cu_3O_x$ tapes and single-grained powders that strongly support the parallel path model are presented. The critical current density of $Bi_2Sr_2Ca_2Cu_3O_x$ tapes can be scaled as a function of magnetic field angle over the temperature range from 15 K to 77 K. Expressions based on classical flux creep are introduced to describe the dependence of the critical current density of $Bi_2Sr_2Ca_2Cu_3O_x$ tapes on the magnetic field and temperature.

DOI: 10.1103/PhysRevB.77.104514 PACS number(s): 84.71.Mn

I. INTRODUCTION

Efforts to develop high-temperature superconducting wires for electric power applications have led to a number of successful demonstration projects[1,2] and commercial applications.[3] Recently, the emphasis has shifted toward the development of $YBa_2Cu_3O_{7-\delta}$ (YBCO-) coated conductors, which has resulted in very high critical current densities (J_c) of over 3 MA/cm^2 in lengths routinely exceeding 300 m.[4] Research in $Bi_2Sr_2Ca_2Cu_3O_x$ (Bi-2223) tapes has also progressed.[5] Their availability in long lengths at relatively low cost makes Bi-2223 tapes currently the choice for large-scale applications. The design of applications and further materials development of Bi-2223 tapes, $Bi_2Sr_2CaCu_2O_x$ (Bi-2212), and YBCO-coated conductors require a detailed understanding of current flow in these conductors and an understanding of the relation between various dissipation mechanisms at different temperatures, magnetic fields, and field orientations.

Improved grain alignment and connectivity in Bi-2223 tapes has been accompanied by the formulation of more advanced models that, with increasing accuracy, describe the limits to the critical current (I_c). The brick-wall model, developed in the early 1990s, describes current flow as if the grains in Bi-2223 tapes are stacked like bricks in a wall.[6,7] In such morphology, current flow from grain to grain is severely hindered along the *ab* planes. Instead, supercurrent crosses from one grain to the next along the *c* direction and dissipation occurs at Josephson-type weak links, both at the grain boundary itself and between the weakly coupled CuO planes within the grains. The railway switch model was developed during the mid-1990s when the quality of Bi-2223 tapes was improved due to a higher degree of grain alignment.[8,9] The authors observed that grains in high-quality tapes are not stacked as bricks in a wall, but are well connected along their *ab* planes. Current does not flow along the *c* axis of the grains, but runs primarily from grain to grain along the *ab* planes. Indeed, the coherence length along the *ab* planes, $\varepsilon_{ab}(0)$, in Bi-2223 is of the order of 1.5 nm,[10] whereas the coherence length in the *c* direction, $\varepsilon_c(0)$, is only on the order of 0.1–1.0 nm.[11,12] Significant current flow along the *c* direction between grains is therefore highly unlikely. Current redistribution occurs through a network of small-angle *c*-axis tilt grain boundaries, resulting in current flow primarily in the *ab* planes, even for current that runs normal to the tape plane in Bi-2223 as has been confirmed by Cho *et al.*[13]

Most models that describe the critical current in Bi-2223 tapes as a function of magnetic field and temperature assume dissipation at low magnetic field to occur within a Josephson network of weak links and dissipation at high magnetic field to result from intragranular flux motion. None of these models accurately predicts the critical current over an extended range of magnetic fields, field angles, and temperatures. The parallel path model assumes that current in Bi-2223 tapes flows through two paths in parallel, with dissipation in each

path occurring through flux creep. A contribution to the overall critical current from current paths that contain Josephson weak links is not excluded and even very likely. These current paths could involve decoupled CuO_2 planes, high-angle grain boundaries, stacking faults, or secondary phases. Since Josephson weak links in general result in a strong reduction of critical current density especially in a magnetic field, current paths that contain Josephson weak links will not significantly contribute to the overall critical current of high-quality Bi-2223 tapes. In order to keep the model as simple as possible, these current paths are not included in the parallel path model. A number of experiments support this picture, and we demonstrate that such a model predicts the dependence of J_c on an extensive range of magnetic fields, field angles, and temperatures. In Sec. II, we introduce the parallel path model and describe the dissipation mechanisms in both types of current paths in Bi-2223 tapes. Different methods to separate the contributions of both current paths are introduced. Clear differences between dissipation mechanisms are revealed by studying the effect of magnetic field and mechanical strain on the critical current density.

In Sec. III, the critical current versus magnetic field behavior of Bi-2223 tapes is related to the direction in which the magnetic field is applied. A scaling of J_c, as a function of magnetic field angle, is demonstrated over the temperature range from 15 K to 77 K by considering the contributions of both individual current paths separately.

In Sec. IV, it is shown that the dissipation in the strongly linked backbone and in the grain boundaries within the weakly linked network are both strongly related to classical flux creep. Expressions for the dependence of the critical current as a function of magnetic field and temperature are introduced.

Finally, in Sec. V, the results are summarized and how Bi-2223 tapes can further be improved is discussed.

II. CURRENT FLOW IN Bi-2223 TAPES

A. Parallel path model

Filaments in multifilamentary Bi-2223 tapes consist of a complex system of long, thin grains that are aligned along their *c* axis within $10°-15°$, on average. The grains are connected over a variety of grain boundary types and form multiple chains along the length of the tape. The most common grain boundaries found in Bi-2223 tapes are those where well-aligned grains have (a) a common *c* axis, but are twisted with respect to their *ab* planes (OABTWIST), (b) edge-on *c*-axis tilt (ECTILT), and (c) small-angle *c*-axis tilt (SCTILT) boundaries[9] (Fig. 1). Grain boundaries in high-temperature superconductors severely limit current transport when the grain boundary angle exceeds about 4°.[14–17] Transport current is limited by flux creep in Bi-2223 along the grain boundary up to an angle of about 8°,[18,19] while Josephson weak links are formed at grain boundaries with angles exceeding about 8°.

It has been shown that transport current in high-quality Bi-2223 tapes flows in part along pathways where grain boundaries form no significant barrier and where dissipation occurs within the grains.[20–23] The grains that make up this

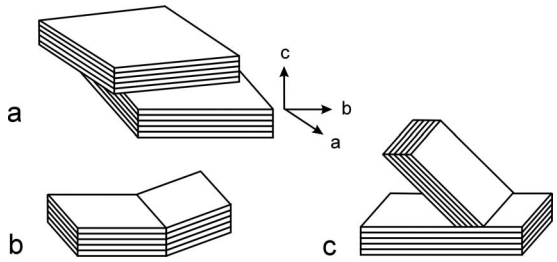

FIG. 1. A representation of grains in Bi-2223 tapes that are connected over distinct grain boundaries: mainly, (a) OABTWIST, (b) ECTILT, and (c) SCTILT.

strongly linked backbone are connected at angles smaller than about 4°. Apart from this backbone, a number of other current paths also contribute to the overall critical current of the tape. The most significant contribution comes from a network of grains that are connected at angles of approximately $4° < \alpha < 8°$, the so-called weakly linked network. Current in this network is limited through intergranular flux motion along these grain boundaries. Current paths that contain grain boundaries larger than 8° do not significantly contribute to the overall current due to their Josephson-like dissipation and therefore are not included in the parallel path model. The overall transport critical current $I_c(B,T,\alpha)$ can then be described as the summation of both contributions:

$$I_c(B,T,\alpha) = I_{cw}(B,T,\alpha) + I_{cs}(B,T,\alpha) \tag{1a}$$

or

$$J_c(B,T,\alpha) = \frac{A_w}{A} J_{cw}(B,T,\alpha) + \frac{A_s}{A} J_{cs}(B,T,\alpha). \tag{1b}$$

In Eqs. (1a) and (1b), $J_{cw}(B,T,\alpha)$ is the critical current density, A_w is the cross section of the weakly linked network, $J_{cs}(B,T,\alpha)$, and A_s represents the same parameter for the strongly linked backbone. The total cross section A of the current path is, of course, the sum of the A_w and A_s. The dependence on magnetic field, temperature, and field angle is determined by the dominant dissipation mechanism of each current path. For instance, weaker pinning of flux at grain boundaries in the weakly linked network compared to intragranular flux pinning in the strongly linked backbone results in a J_{cw} dependence on magnetic field that is steeper than that of J_{cs}. This results in a typical double step in the overall critical current density as a function of magnetic field when the magnetic field is applied perpendicular to the tape surface[24] (see Fig. 2). All Bi-2223 tapes that are part of this research have been produced by the powder-in-tube method. Here, the critical current density is measured with a transport current at an electric field criterion of 1 μV/cm and the critical current density is obtained by dividing I_c by the overall cross section of the Bi-2223 core. The tape (sample B-1) consists of 85 filaments and a silver matrix, a cross section of the ceramic core of 0.3 mm, and has a self-field I_c at 77 K of about 36 A. The critical current density of the weakly linked network is strongly reduced at intermediate magnetic fields, whereas the critical current density of the strongly linked backbone decreases significantly only at higher magnetic

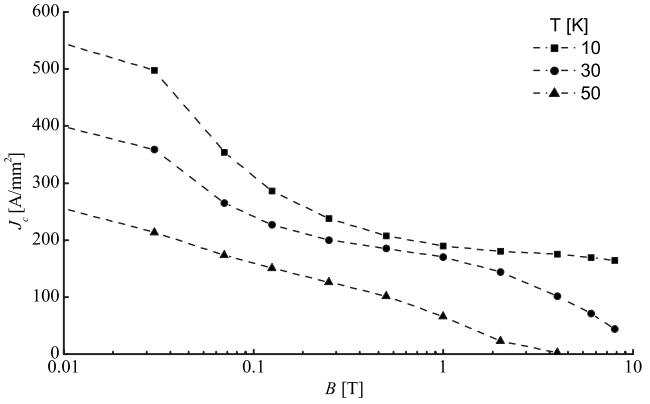

FIG. 2. Transport critical current density of a Bi-2223 tape (B-1) as a function of magnetic field at various temperatures. The magnetic field is applied perpendicular to the tape surface. The dashed lines are guides for the eye.

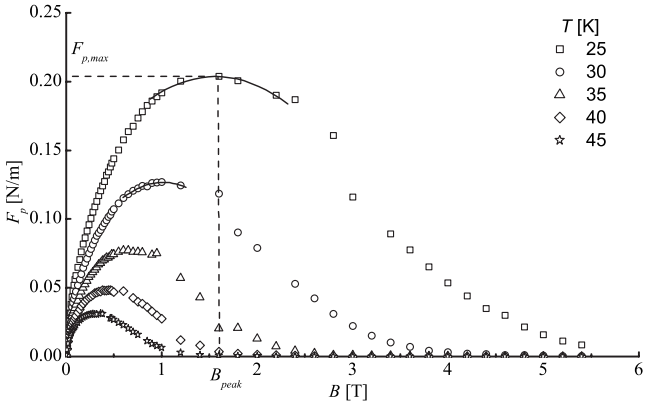

FIG. 3. Macroscopic pinning force as a function of magnetic field at various temperatures of tape B-2. The magnetic field is applied perpendicular to the tape surface. The solid lines are a second-order polynomial fit around the maximum of the pinning force.

fields. Transport current below I_c is divided between the current paths such that dissipation in both types of current paths is comparable.

B. Dissipation in high magnetic fields

To understand dissipation in Bi-2223 tapes, it is important to study dissipation processes both in the weakly linked network and in the strongly linked backbone. Measuring the contributions of both current paths separately is not straightforward, since both are contained within the overall critical current of the tape. Fortunately, a magnetic field affects J_{cs} and J_{cw} differently. The contribution J_{cw} of the weakly linked network to J_c diminishes at intermediate magnetic fields and completely vanishes at higher magnetic fields, where only the contribution J_{cs} of the strongly linked backbone remains. Intragranular flux motion in the strongly linked backbone can thus be studied directly at high magnetic fields.

When dissipation occurs through intragranular flux motion and when the pinning potential is a logarithmic function of current, the critical current density decays exponentially with magnetic field.[25] An exponential decay of J_c has been observed in Bi-2223 tapes at higher magnetic fields by a number of authors.[9,20,26] The temperature and magnetic field dependence of the overall J_c of a Bi-2223 tape in higher magnetic fields, and thus the critical current density of the strongly linked backbone, can as a first approximation described by

$$J_{cs}(B,T) = J_{cs}(0,T)\exp\left(-\frac{B}{B_{\text{peak}}(T)}\right). \tag{2}$$

This empirical relation is a rough estimate of the critical current density at high magnetic fields which will be discussed in the second part of this paper, but all its parameters can be directly obtained from experimental data. With this approximation, we can describe current flow without going right away into details about the underlying dissipation mechanisms. The temperature-dependent characteristic field $B_{\text{peak}}(T)$ in Eq. (2) reflects the pinning force in the strongly linked backbone. Its value is obtained directly from experimental results by deriving the macroscopic pinning force (F_p). The macroscopic pinning force was introduced by Kramer[27] to describe the pinning properties of metallic type-II superconductors and is defined as

$$F_p = |J_c \times B|. \tag{3}$$

F_p shows a maximum as a function of applied magnetic field, as shown in Fig. 3. Here, the critical current density of the sample is derived from its dc magnetization using the critical-state model,[28] where J_c a linear function of the irreversible magnetization. The dc magnetization of the 4-mm-long sections of the tape is measured with a superconducting quantum interference device (SQUID) magnetometer. In the original Kramer analysis, flux motion occurs by flux-line depinning at fields below the peak field (B_{peak}) (determined by a second-order polynomial fit around the maximum) and by synchronous shear of the flux-line lattice above the peak field. However, in this paper, the position of the peak is used more generally to select a temperature-dependent scaling field for analyzing the data.

When J_{cs} [Eq. (2)] is normalized to the maximum pinning force $F_{p\,\max}$ at the peak field B_{peak}, we obtain the empirical relation for the critical current density of the strongly linked backbone is obtained[29] as

$$J_{cs}(B,T) = \frac{F_{p\,\max}(T)}{B_{\text{peak}}(T)}\exp\left(1-\frac{B}{B_{\text{peak}}(T)}\right). \tag{4}$$

Dissipation in the strongly linked backbone is described separately by use of the above procedure. The two fitting parameters B_{peak} and $F_{p\,\max}$ in Eq. (4) are completely defined by the macroscopic pinning force (see Fig. 3) and obtained directly from the data. Figure 4 shows the magnetic field dependence of the overall J_c of a Bi-2223 tape that is derived from the dc magnetization at a range of temperatures. The tape (B-2) consists of 55 filaments, a cross section of the ceramic core of 0.3 mm, a silver matrix, and a self-field I_c at 77 K of about 65 A. The J_c that is obtained from dc magne-

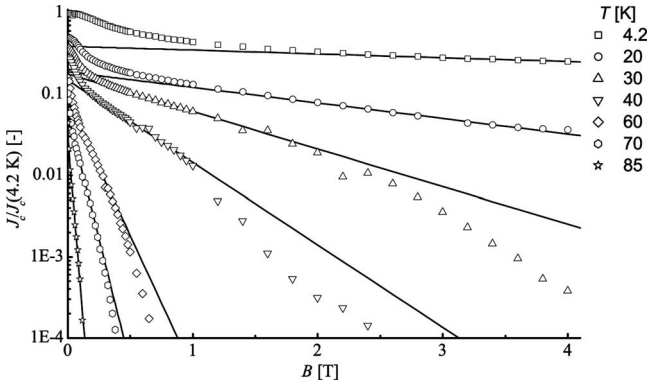

FIG. 4. Normalized critical current density of Bi-2223 tape B-2 measured with dc magnetization as a function of magnetic field at various temperatures. The magnetic field is applied perpendicular to the tape surface. The solid lines are fits to Eq. (4).

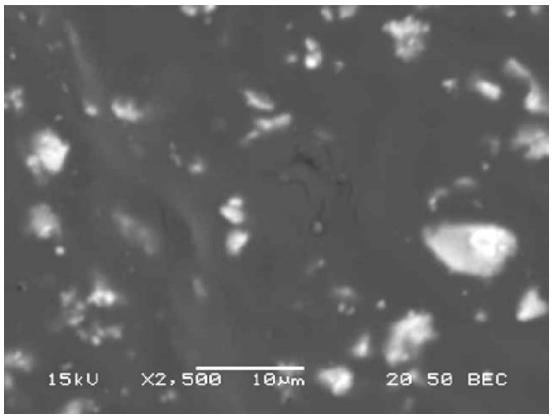

FIG. 5. Scanning-electron micrograph of aligned grains that were extracted from a Bi-2223 tape (B-2).

tization behaves similarly as a function of magnetic field when compared to the J_c as is obtained from transport measurements. This confirms that there exist chains of strongly linked grains that are connected over the entire length of the sample and that a simple model based on weakly linked grains does not apply. Note the difference in characteristic fields between the J_c value obtained from dc magnetization and that obtained from transport measurements, which is due to the difference in electric field between both measurement procedures. The solid lines represent the exponential decay of J_c with field [Eq. (4)] and show a reasonable fit to the measured J_c at high magnetic field. The contribution of the weakly linked network to the overall J_c is observed at low magnetic fields, where the actual J_c value is substantially higher than that predicted by Eq. (4). A deviation between the exponential field dependence of J_{cs} and the observed critical current density is evident for low current and high magnetic fields, and is due to the over-simplification inherent in Eq. (4). A deviation from the empirical relation given by Eq. (2) where Eq. (4) is derived from is clearly observed. A more detailed relation that is based on classical flux creep will be introduced in Sec. IV. The approximation here does influence the separation of the contributions of both current paths somewhat, but has a negligible effect on the results presented in the remainder of this paper.

C. Aligned single-grained Bi-2223 powder

It was demonstrated in the previous section that intragranular flux creep is the dominant dissipation mechanism within the strongly linked backbone in Bi-2223 tapes. It is possible to separate J_{cs} from the overall J_c of the tape by using an external magnetic field to suppress the critical current density of the weakly linked network.

Intragranular dissipation can also be studied directly in single-grained samples where no grain boundaries are present. Dissipation within the strongly linked backbone can thus be studied in single-grained powders extracted from a Bi-2223 tape by measuring J_c with dc magnetization. Previous studies on single-grained Bi-2223 powder showed a significant reduction in J_c at low magnetic field, but no direct comparison between intact tape and ground powder could be made.[30–32] The magnetic field dependence of J_c in layered high-temperature superconductors such as Bi-2223 depends strongly on the angle at which the magnetic field is applied. This is due to the large anisotropy in J_c along the c axis, compared to J_c in the ab plane[33] (see Sec. III). A direct comparison between the field and temperature dependence of the J_c of a tape and of a single-grained powder extracted from the tape is possible only when the powder has a grain alignment that is comparable to that of the tape.

In this study, a single-grained powder was extracted from a mono-core Bi-2223 tape by grinding the core and removing remaining clusters of connected grains from the powder by filtering out particles larger than 10 μm.[34] The resulting powder had a grain size smaller than 10 μm, which is well below the average size of grains in Bi-2223 tapes. It cannot be guaranteed that the powder does not include any grain boundaries, although their number is strongly reduced from that in a tape. Grain alignment was then introduced by mixing the powder with diluted epoxy and pressing the resulting solution on a glass plate. This procedure aligned the small plate-like grains with their ab planes parallel to the glass plate. After the epoxy was cured, a thin sample was obtained, containing c-axis-aligned Bi-2223 grains (Fig. 5). This film was cut into multiple round disks with a diameter of $\sim$5 mm that were stacked on top of each other to increase the sample volume in the dc magnetization measurement. A high degree of c-axis alignment of the grains in the powder is important to be able to make a comparison with a tape. The critical current density of the powder will decrease more slowly at high magnetic field when the alignment of the powder is not comparable to that of the tape. The effective magnetic field component parallel to the c axis of the grains in that case will be smaller in the powder than in the tape. The high degree of c-axis alignment in the powder used in this study follows directly from its behavior in high magnetic field, comparable to that of a tape, as will be shown later.

The critical current densities of the Bi-2223 tape and that of the aligned powder were measured with dc magnetization (Fig. 6), with the magnetic field applied perpendicularly to the surface of the tape and the powder stack (along the c axis of the grains). The difference in sample size between powder

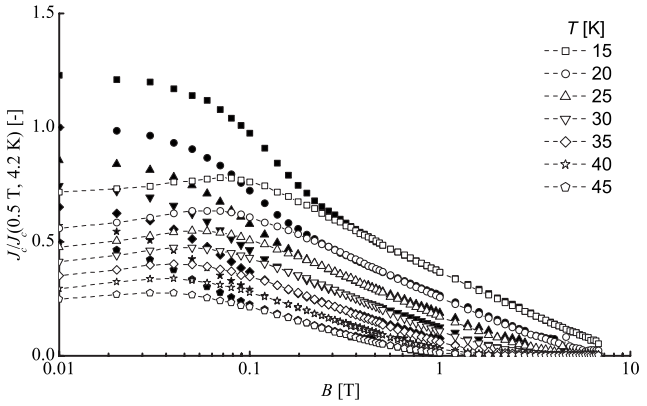

FIG. 6. Critical current density as a function of magnetic field of Bi-2223 tape B-2 (solid symbols) and the powder extracted from the tape (open symbols) at various temperatures. Open and solid symbols of the same type correspond to the same temperature. The critical current density is normalized to its value at 4.2 K and 0.5 T. The dashed lines are guides for the eye.

and tape was taken into account by normalizing the critical current density to its value at 4.2 K and at a magnetic field of 0.5 T. The weakly linked network in the tape carries no current at this field. An absolute value for the critical current density of the powder cannot be provided since the exact sample size is unknown. A comparison between the critical current density of the tape (solid symbols) and that of the powder (open symbols) shows that the magnetic field dependence of both J_c values is comparable above a temperature-dependent minimum magnetic field. The critical current density of the powder at low magnetic field is indeed lower than that of the tape, due to the absence of a weakly linked network.

The dissipation in the strongly linked backbone of the tape that in the aligned powder is further compared by means of the macroscopic pinning force as well. The temperature dependence of the magnetic fields at which the macroscopic pinning force is maximum (B_{peak}) in both tape and powder is compared in Fig. 7. As expected, the intragranular pinning

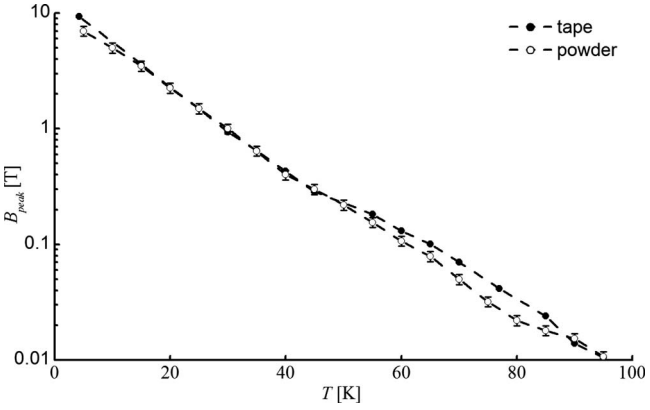

FIG. 7. Temperature dependence of the field at which the macroscopic pinning force is maximum (B_{peak}) of a Bi-2223 tape and the powder extracted from the tape. The lines are guides for the eye.

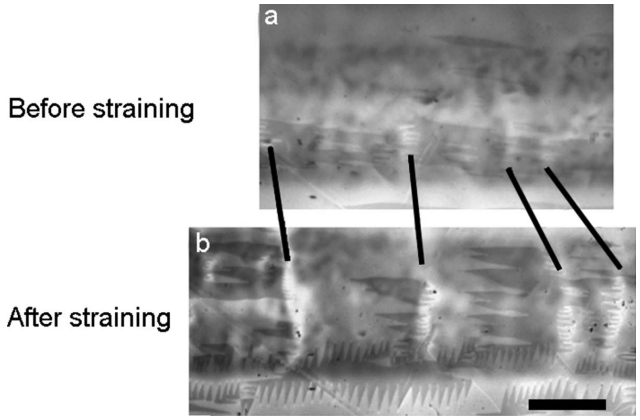

FIG. 8. (a) MO image of part of a Bi-2223 filament (oriented horizontally) in tape B-3 before axial strain is applied. The filament is partly shielded from the external magnetic field of 25 mT (dark areas). (b) Less dense areas form filament-wide cracks after strain is applied (bright areas), starting at a strain of ~0.6%. The scale bar represents 125 μm.

properties are not changed by grinding the tape into a powder. The values of B_{peak} are comparable for the tape and the powder and have a comparable temperature dependence. The mechanical grinding does not influence the pinning properties of the powder by introducing additional pinning sites. Damage from grinding is expected to occur on a much larger length scale than the coherence length of 1–2 nm and will therefore only limit the critical current density by breaking the ceramic core.

The results presented here strongly support the parallel path model. The comparable dependences on magnetic field of J_c in the powder and that in the tape at higher magnetic fields confirms that chains of well-connected grains exist in Bi-2223 tapes, in which dissipation occurs not at grain boundaries, but rather inside the grains. A network of grains that are connected at intermediate angle contributes to the overall J_c of the tape only in relatively low magnetic fields.

D. Effect of strain on the critical current

The filaments in Bi-2223 tapes can be severely damaged by mechanical strain. It is well known that the critical current density of the tape degrades irreversibly when an applied axial strain exceeds the irreversible strain limit (ε_{irr}).[35–38] Microscopy shows that this degradation occurs due to damage to the grain structure on both a submillimeter length scale, observed with magneto-optical imaging (MOI),[39–41] as well as on a finer micrometer length scale, observed in scanning-electron-microscopy (SEM) studies.[42,43]

Defects on a submillimeter length scale occur in the filaments of Bi-2223 tapes at strains much larger than ε_{irr}. They are formed at locations where the microstructure is less dense due to sausaging or other preexisting inhomogeneities. An example of these filament-wide cracks that develop at high strain is shown in Fig. 8. Cracks that span the width of the Bi-2223 filaments were observed at an applied strain of 0.6% (1.5 times ε_{irr}). The tape (B-3) consists of 65 filaments,

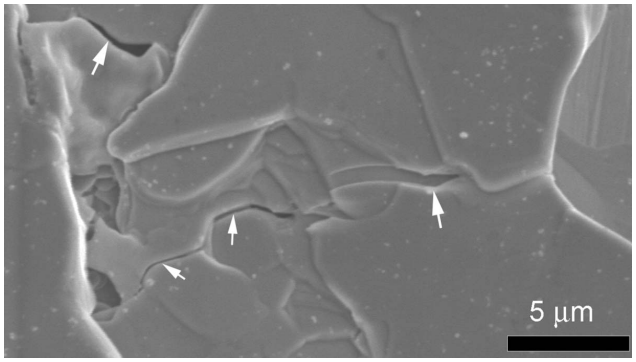

FIG. 9. SEM image of the grain structure of Bi-2223 tape B-4 showing cracks (arrows) after tensile strain exceeding ε_{irr} is applied *in situ*. The exact amount of applied strain is unknown, due to the partial etching of the tape surface.

a cross section of the ceramic core of 0.15 mm, a silver matrix, and a self-field I_c at 77 K of about 20 A. The magneto-optical image shows that an applied magnetic field of 25 mT partly penetrates the grain structure at these locations even before strain is applied [Fig. 8(a)]. These locations of relatively easy flux penetration in the filaments form cracks at high strain [Fig. 8(b)].

Although the filament-wide cracks that are observed with magneto-optical imaging will certainly block a transport current, they are not responsible for the initial degradation in J_c when the irreversible strain limit is exceeded. The damage to the grain structure that is responsible for this initial degradation of J_c occurs on a much finer micrometer scale, far below the resolution of MOI. Microcracks form at strains exceeding ε_{irr} before filament-wide cracks appear, as observed *in situ* by SEM (Fig. 9). The tape (B-4) consists of 55 filaments, a cross section of the ceramic core of 0.39 mm, a silver matrix and a self-field I_c at 77 K of about 135 A.

Both the weakly linked network and the strongly linked backbone are affected by mechanical strain. Since both types of current paths differ in grain structure (grains connected at low angle in the strongly linked backbone versus grains connected at angles up to 8° in the weakly linked network), axial strain is unlikely to affect them equally.[44] According to the parallel path model, a difference in strain sensitivity between both current paths would be revealed when J_c is measured as a function of axial strain in the presence of a magnetic field. In that case, the decrease in J_c with strain (exceeding ε_{irr}) at low magnetic field would be different from the decrease in J_c at high magnetic field. Exactly this behavior was observed when the transport J_c of a Bi-2223 tape was measured as a function of axial strain ($\varepsilon_{irr} \sim 0.5\%$ for this particular sample) and a magnetic field applied perpendicular to the tape surface. The tape (B-5) consists of 19 filaments, a silver matrix, and a self-field I_c at 77 K of about 30 A. For example, the critical current at a strain of 0.83% degraded by ~75% in self-field, but only by ~40% at 280 mT [see Fig. 10(a)]. The difference in strain sensitivity is even more apparent from the degradation in n value [the slope in the curve for $\log(E)$ vs $\log(J)$; see Sec. IV] [Fig. 10(b)]; the degradation in self-field was 65%, compared to only 10% at 280 mT.

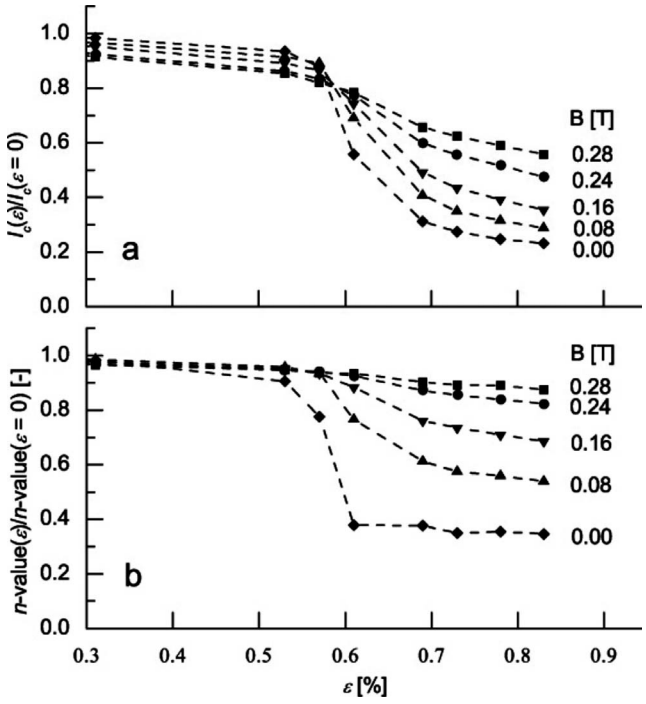

FIG. 10. (a) Normalized critical current of Bi-2223 tape B-5 as a function of axial strain at 77 K for different magnetic fields applied perpendicular to the wide side of the tape, showing a greater effect of strain at low magnetic fields. (b) Normalized n-value as a function of axial strain and magnetic field.

From these results it can be concluded that axial strain exceeding ε_{irr} affects high-angle grain boundaries more than grains that are connected at low angle, which can be seen as further support for the parallel path model. High-angle grain boundaries are not only characterized by weaker flux pinning, but are also mechanically weaker than low-angle grain boundaries, as evidenced by a faster J_c decrease with strain at low magnetic fields compared to that at high magnetic fields.

III. MAGNETIC FIELD ANGLE DEPENDENCE OF J_c

The critical current density of Bi-2223 tapes depends not only on the applied magnetic field, but also on the angle at which the field is applied with respect to the crystalline axis. Magnetic flux pinning is much stronger when the field is applied parallel to the tape surface, and dissipation depends largely on the magnetic field component perpendicular to the tape.

Large anisotropy in combination with a small coherence length results in a weak coupling between the CuO_2 planes of layered high-temperature superconductors within a wide temperature range where the spacing between the CuO_2 planes is larger than the coherence length normal to the planes.[11,12,45–47] The normal regions between the planes act as strong pinning centers for flux lines oriented along the *ab* planes[33] (referred to as the parallel magnetic field direction), whereas the pinning of flux lines perpendicular to the *ab* planes (parallel to the *c* axis of the grains and referred to as

the perpendicular magnetic field direction) is much weaker and depends on the landscape of defects that act as pinning centers.[48] The strong intrinsic flux pinning along the *ab* planes results in a J_c of thin films and single crystals that is almost independent of magnetic field for fields applied along the *ab* plane.

Since Bi-2223 tapes consist of a large number of platelike grains that are aligned within $\sim 10° - 15°$ following a Gaussian distribution,[7] a magnetic field applied parallel to the tape plane will still result in a small magnetic field component parallel to the *c* axis of most grains.[49] This component of the magnetic field parallel to the *c* axis of the grains B_{eff} causes the reduction in J_c with magnetic field in Bi-2223 tapes.[8,9,50–52]

Until now, modeling the dependence of J_c on magnetic field angle over a wide temperature range has not been successful, even when the effective magnetic field component parallel to the *c* axis of the grains is regarded as the driving force behind dissipation in Bi-2223 tapes. According to the parallel path model, current flows in two types of current paths, with clear differences in grain structure (and thus grain alignment). Grains in the strongly linked backbone are better aligned than grains in the weakly linked network, resulting in a difference in B_{eff} for both current paths. Dissipation in these current paths also occurs at different locations (at grain boundaries for the weakly linked network and within the grains for the strongly linked backbone). A successful scaling of J_c on magnetic field angle (by calculating the effective magnetic field component responsible for dissipation) can be achieved only when both types of current path in Bi-2223 tapes are regarded separately, an approach that was not taken in previous investigations.

The dependence of J_c of Bi-2223 tapes on magnetic field angle along the lines of the parallel path model is analyzed by measuring J_c for magnetic fields applied parallel and perpendicular to the tape surface. The critical current density is extracted from the dc magnetization and is normalized to its self-field value at 4.2 K. These data are shown as a function of magnetic field in Fig. 11 for both field directions at temperatures between 15 K and 45 K. The anisotropy in magnetic flux pinning is evidenced by a much stronger field dependence of J_c when the magnetic field is applied perpendicular to the tape surface (solid symbols), compared to when it is applied parallel to the tape surface (open symbols).

Scaling the $J_c(B)$ dependence at high magnetic field for both parallel and perpendicular magnetic field directions is straightforward, since only the strongly linked backbone carries current at high field. The effective magnetic field component parallel to the *c* axis of the grains (B_{eff}) that applies to the strongly linked backbone is thus entirely determined by the average grain alignment of the strongly linked backbone and the dissipation mechanism in this current path. B_{eff} is nearly equal to the applied field when the magnetic field is applied perpendicular to the tape surface, and $B_{\text{eff}}=B/b_{scs}$ when the field is applied parallel to the tape surface. The scaling factor b_{scs} is determined from the macroscopic pinning force and is equal to the fraction of the peak field (B_{peak}) for both magnetic field directions:

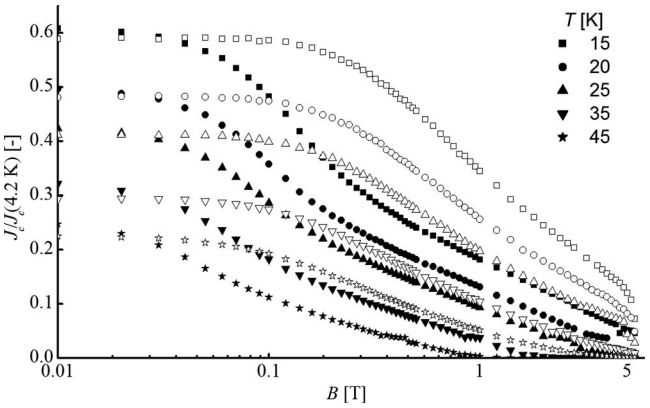

FIG. 11. Normalized critical current density obtained from dc magnetization of Bi-2223 tape B-2 as a function of magnetic field applied parallel (open symbols) and perpendicular (solid symbols) to the tape surface, at different temperatures. Open and solid symbols of the same type correspond to the same temperature. The critical current density is normalized to its value at 4.2 K.

$$b_{scs} = \frac{B_{\text{peak},\parallel}}{B_{\text{peak},\perp}}. \tag{5}$$

Here, $B_{\text{peak},\parallel}$ is the magnetic field where the macroscopic pinning force is a maximum for a parallel applied magnetic field and $B_{\text{peak},\perp}$ is the field for a perpendicular applied field. The critical current density as a function of B_{eff} at high magnetic field (i.e., completely carried by the strongly linked backbone) coincides for both field directions over a large temperature range (see Fig. 12).

A large deviation between $J_c(B_{\text{eff}})$ for both field directions is observed at low magnetic field, where the weakly linked network significantly contributes to the overall J_c. The difference in average grain alignment and the difference in dissipation mechanism results in a different B_{eff} of the weakly

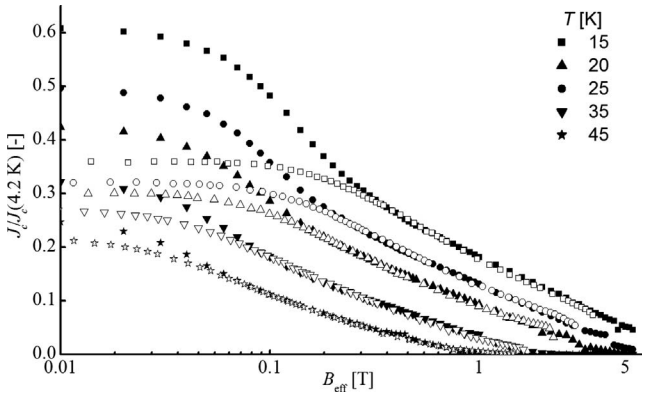

FIG. 12. Normalized $J_c(B_{\text{eff}})$ for magnetic field applied parallel (open symbols, $B_{\text{eff}}=B/b_{scs}$) and perpendicular (solid symbols, $B_{\text{eff}}=B$) to the tape surface of tape B-2 at different temperatures. Open and solid symbols of the same type correspond to the same temperature. The critical current density is normalized to its self-field value at 4.2 K.

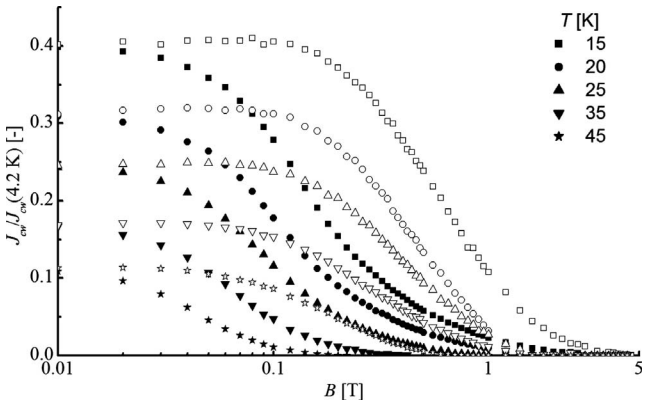

FIG. 13. Critical current density of the weakly linked network as a function of magnetic field applied parallel (open symbols) and perpendicular (solid symbols) to the wide side of tape B-2, at different temperatures. Open and solid symbols of the same type correspond to the same temperature. The critical current density is normalized to its self-field value at 4.2 K.

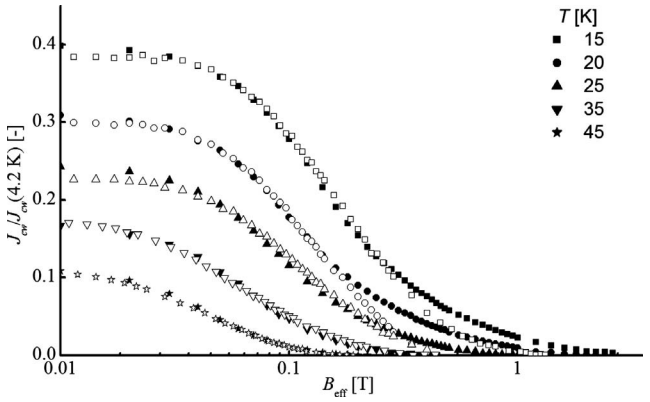

FIG. 14. Normalized critical current density of the weakly linked network as a function of effective magnetic field component (B_{eff}) at different temperatures for magnetic fields applied parallel (open symbols, $B_{\mathrm{eff}}=B/b_{scw}$) and perpendicular (solid symbols, $B_{\mathrm{eff}}=B$) to the surface of tape 2. Open and solid symbols of the same type correspond to the same temperature.

linked network when compared to that of the strongly linked backbone.

The dependence of the dissipation in the weakly linked network on magnetic field direction is determined by determining the scaling factor b_{scw}, which defines $B_{\mathrm{eff}}=B/b_{scw}$ for this current path. The critical current density J_{cw} of the weakly linked network is obtained by subtracting the critical current density J_{cs} of the strongly linked backbone [Eq. (4)] from the overall J_c of the tape. A clear difference in magnetic field dependence of J_{cw} is shown in Fig. 13 for magnetic fields applied parallel and perpendicular to the surface of the tape. A less sensitive $J_{cw}(B)$ dependence on applied magnetic field is measured when the magnetic field is applied parallel to the tape surface, compared to perpendicular to the tape surface; a behavior similar to that of the strongly linked backbone. A close correlation in J_{cw} for both field directions is found (Fig. 14) when J_{cw} is plotted as a function of effective magnetic field component (B_{eff} is approximately equal to the applied magnetic field when it is applied perpendicular to the tape surface, and $B_{\mathrm{eff}}=B/b_{scw}$ when the magnetic field is applied parallel to the tape surface). The scaling factor b_{scw} is chosen such that $J_{cw}(B)$ coincides for both magnetic field directions. Only a relatively small deviation is found at intermediate magnetic fields, presumably due to the incomplete separation of the contribution of the weakly linked network form the overall J_c, since Eq. (4) is an approximation of J_{cs}. This incomplete separation has no significant influence on the value of b_{scw}.

Dissipation in the weakly linked network and dissipation in the strongly linked backbone are not equally sensitive to a magnetic field that is applied parallel to the tape surface. The scaling factors b_{scs} and b_{scw} that define B_{eff} for both current paths are compared in Fig. 15 and show distinct differences. The scaling factor b_{scw} is larger, approximately 3.8 ± 0.3, and is independent of temperature. A similar temperature independence is measured for the strongly linked backbone at temperatures above 50 K. Even though the strongly linked backbone has a higher degree of grain alignment, its dissipation mechanism is more sensitive to a parallel applied magnetic field than is the dissipation mechanism of the weakly linked network. Below 50 K, b_{scs} is temperature dependent and varies from approximately 3.0 at 50 K to 1.4 when the temperature is reduced to 15 K. This behavior indicates that dissipation in the strongly linked backbone becomes more sensitive to parallel magnetic field at reduced temperatures and becomes almost independent of magnetic field angle at 15 K.

The relatively small difference in B_{eff} between the weakly linked network and the strongly linked backbone above 50 K explains why a field angle scaling of the overall $J_c(B)$ has been successful at 77 K when both current paths are treated as equal.[53,54] Here it is demonstrated that such a scaling will be unsuccessful at temperatures below 50 K when current flow in Bi-2223 tapes is described along the lines of a single current path. The clear differences in current paths must be taken into account for such a scaling to be successful, which strongly supports the parallel path model.

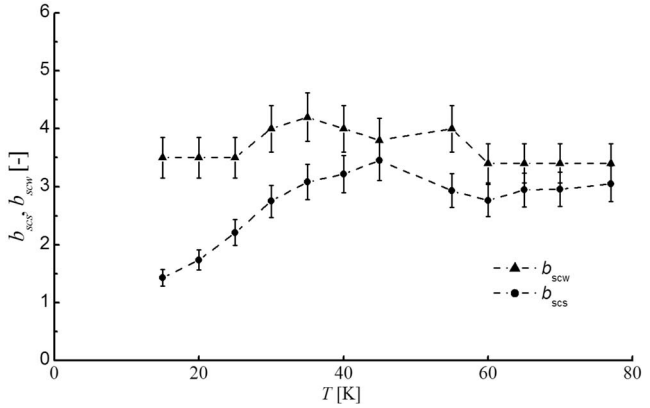

FIG. 15. Scaling factor b_{scs} for the strongly linked backbone and b_{scw} for the weakly linked network as a function of temperature. The dashed lines are a guide to the eye.

IV. FLUX MOTION IN Bi-2223 TAPES

A. Classical flux-creep theory

The critical current density for a chain of well-connected Bi-2223 grains is limited by intragranular flux motion, as long as the grain boundary angles do not exceed 4°.[14–17] The flux lines are pinned within the grains by a landscape of defects that can be described by a pinning potential $U(B,T,J)$ that depends on magnetic field, temperature, and current density. A Lorenz-force-driven depinning of the flux lines results in flux motion, which in turn results in an electric field E.

Flux lines that become depinned generate an electric field defined by $E=Bv$. When thermal activation over a pinning barrier is causing the flux motion, the velocity v can be written as[55]

$$v = v_0 \ e^{-U(B,T,J)/kT}. \tag{6}$$

This determines the electric field as

$$E(B,T,J) = E_0(B)e^{(-U(B,T,J)/kT)} \tag{7}$$

and

$$E_0(B) = v_0 B = \omega_0 L B. \tag{8}$$

In Eq. (8), ω_0 is the attempt frequency and L the hopping distance over which flux lines move when they become depinned. The pinning potential of a superconductor can be obtained by measuring the magnetic relaxation of the critical current density.[25] A logarithmic dependence of the pinning potential on current density was found for Bi-2223 tapes[56–58]:

$$U(B,T,J) = U_0(B,T)\ln\left(\frac{J_c(0,T)}{J}\right). \tag{9}$$

The pinning potential vanishes when the current density becomes equal to the critical current density $J_c(0,T)$ at zero applied magnetic field. The dependence of the prefactor U_0 on temperature and magnetic field has the following form[59]:

$$U_0(B,T) = kT\left(\frac{B_{\rm irr}(T)}{B}\right)^n. \tag{10}$$

The irreversibility field $B_{\rm irr}(T)$ is defined as the magnetic field at which the flux line lattice changes from a vortex solid to a vortex liquid, resulting in flux flow and a large electric field over the superconductor. This is a measure for the flux pinning strength, which is related, but not equal, to $B_{\rm peak}$ in the macroscopic pinning force. Inserting Eqs. (9) and (10) into Eq. (7) provides an equation for the electric field $E(J,B,T)$ and an equation for the critical current density $J_c(B,T)$ by setting $E=E_c$ at $J=J_c$:

$$E(B,T,J) = E_0(B)\left(\frac{J}{J_c}\right)^{(B_{\rm irr}(T)/B)^n} \tag{11}$$

and

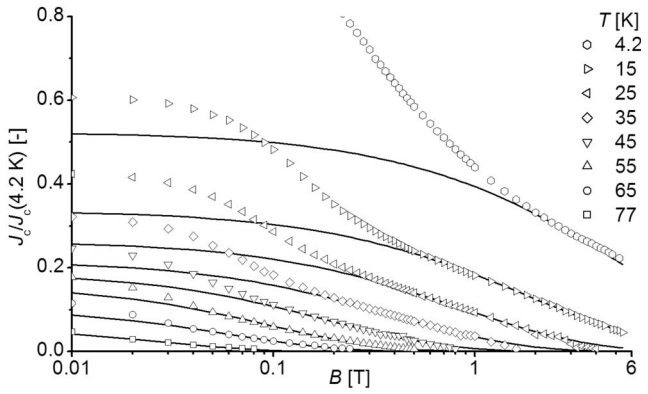

FIG. 16. Critical current density of Bi-2223 tape B-2 measured with dc magnetization as a function of magnetic field. The critical current density is normalized to its value at 4.2 K. The magnetic field is applied perpendicular to the tape surface. The lines represent J_{cs} according to classical flux-creep theory [Eq. (12)].

$$J_c(B,T) = J_c(0,T)\exp\left[-\left(\frac{B}{B_{\rm irr}(T)}\right)^n \ln\left(\frac{E_0(B)}{E_c}\right)\right]. \tag{12}$$

Equations (11) and (12) describe the electric field and the critical current density of a superconductor when dissipation occurs through thermally activated intragranular flux creep, such as in the strongly linked backbone of Bi-2223 tapes and within a single-grained Bi-2223 powder. The magnetic field dependence of the critical current density, according to Eq. (12), is dominated by the exponential term and simplifies to Eq. (4). The term $[B_{\rm irr}(T)/B]^n$ in Eq. (11) corresponds to the power in the E-J relation and is the slope of the $\log(E)$-$\log(J)$ curve.

B. Intragranular flux motion in Bi-2223

The parallel path model is capable of describing current flow in Bi-2223 tapes, as was demonstrated by a number of experiments in Secs. II and III. The experiments indeed indicate that current can be modeled to flow in two parallel paths. Furthermore, there is clear evidence that dissipation in high magnetic fields is caused by intragranular flux motion. Here, it is determined whether intragranular flux motion in Bi-2223 tapes can be described by classical flux-creep theory [Eq. (12)].

The critical current density of a Bi-2223 tape extracted from the dc magnetization as a function of magnetic field at various temperatures is shown in Fig. 16. The dependence of J_c on magnetic field can be described accurately by classical flux creep in high magnetic fields [Eq. (12), solid lines]. The irreversibility field $B_{\rm irr}$ is substituted by $B_{{\rm irr},s}$ to indicate that this is the scaling field of the strongly linked backbone. Table I lists the parameter values of Eq. (12) that apply to the Bi-2223 tape, while the temperature dependence of $J_{cs}(0,T)$ is shown in Fig. 21(a) and that of $B_{{\rm irr},s}(T)$ in Fig. 21(b). A value of 0.01 is taken for the velocity v_0 in Eq. (8). The deviation between model and measurement at low magnetic fields in Fig. 16 can be explained by the contribution of the weakly linked network to the overall J_c.

TABLE I. Parameter values of Eqs. (12) and (14) for tape B-2.

	v_0 [m/s]	E_c [V/m]	n_w [–]	n_s [–]	J_{cw}, $J_{cs}(0,T)$ [A/mm^2]	$B_{\mathrm{irr},w}B_{\mathrm{irr},s}(T)$ [T]
Bi-2223 transport	0.01	10^{-4}	0.45	1.23	Fig. 21(a)	Fig. 21(b)
Bi-2223 dc-magnetization	0.01	10^{-5}	0.96	0.52	Fig. 21(a)	Fig. 21(b)

The critical current density of the strongly linked backbone of Bi-2223 tapes can also be described by classical flux-creep theory when J_c is measured with a transport current (Fig. 17). Classical flux creep [Eq. (12)] describes J_c in the magnetic field region where the weakly linked network no longer contributes to the overall critical current (parameters listed in Table I), which is above 1 T at 4.2 K for a transport measurement. The weakly linked network carries a significant part of the transport current at low field.

The hypothesis that classical flux creep is responsible for the dissipation in the strongly linked backbone is supported by the current-voltage characteristics that were measured around the superconducting transition at $E=E_c$ of the tape (Fig. 18). The electric field across the superconductor is well described by the power-law dependence [Eq. (11)] around the electric field criterion of 10^{-4} V/m at high magnetic field, where the weakly linked network no longer contributes to the overall critical current density. The dashed horizontal line in the figure is the voltage criterion of $E_c=10^{-4}$ V/m for which the critical current density is defined.

C. Intergranular flux motion in Bi-2223 tapes

Grain boundaries present in the microstructure of various high-temperature superconductors suppress a supercurrent when the grain boundary angle exceeds about 4°.[14–17] The strain fields that are formed due to the lattice mismatch at the boundary lower the effective cross section of the current path over the grain boundary. The strain fields start to overlap at a grain boundary angle exceeding about 8° (Refs. 18 and 19), at which angle the grain boundary becomes weakly linked and Josephson behavior is measured.[15,60] Dissipation at low magnetic field is therefore often described along the lines of a Josephson coupled network of grains.[61–63] A widely used expression for J_c of a network of weakly coupled grains is given by[64,65]

$$J_c(B,T) = \frac{J_c(0,T)}{1+\left(\frac{|B|}{B_0(T)}\right)^{\beta}}. \tag{13}$$

The characteristic field of the weak links is presented by B_0, and β reflects the geometry of the weak links.[66] When the weak links have an elliptical cross section, β has a value of 3/2 and the magnetic field dependence is the same as in the case of an Airy diffraction pattern. In case of rectangular junctions, one obtains $\beta=1$ when the field that penetrates the weak links is within a few degrees of being parallel to one of the junction edges. For other field orientations, $\beta=2$.

According to the parallel path model, the weakly linked network in Bi-2223 tapes consists of grains that are connected at angles below 8° and no Josephson behavior is expected. A different description of dissipation in the weakly linked network is obtained when one assumes coupling between intergranular and intragranular flux lines.[67–69] Abrikosov vortices with highly anisotropic Josephson cores (AJ vortices) at grain boundaries are pinned at defects that are formed mainly by strain fields. Intergranular flux pinning at boundary defects is not the only pinning mechanism. A strong electromagnetic interaction between the intergranular AJ vortices and the intragranular Abrikosov vortices exists,

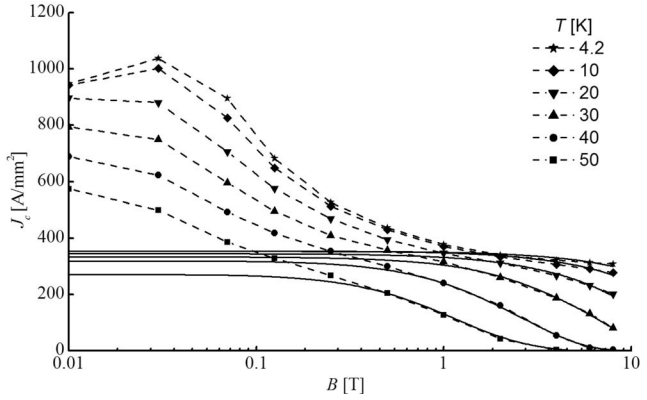

FIG. 17. Transport J_c of Bi-2223 tape B-2 measured as a function of magnetic field applied perpendicular to the tape surface. The solid lines represent the critical current density of the strongly linked backbone according to classical flux-creep theory [Eq. (12)]. The dashed lines are a guide to the eye.

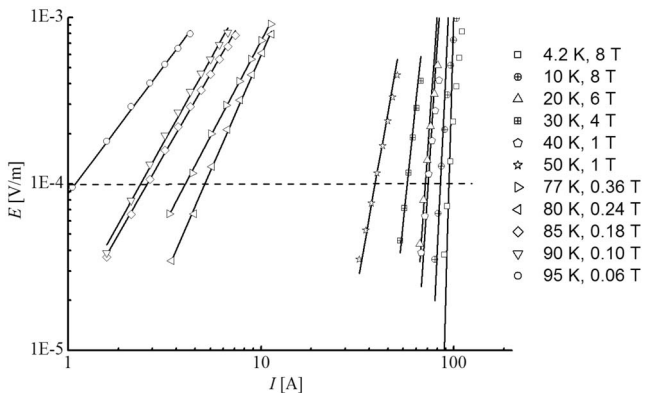

FIG. 18. $E(I)$ characteristics at high magnetic fields of Bi-2223 tape B-2, measured at different temperatures. The solid lines represent the $E(I)$ characteristics according to classical flux creep [Eq. (11)]. The dashed line is the voltage criterion at which the critical current is defined.

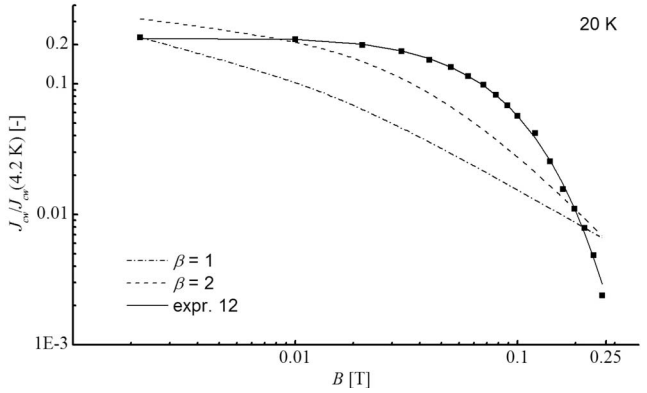

FIG. 19. Normalized critical current density of the weakly linked network of Bi-2223 tape B-2 that is measured with dc magnetization at 20 K. The magnetic field is applied perpendicular to the wide side of the tape. J_{cw} is obtained by subtracting J_c of the aligned powder from that of the tape from which the powder was extracted. The critical current density is described according to a network of Josephson weak links [Eq. (13)], with $\beta=1$ and $\beta=2$, and according to classical flux-creep theory [Eq. (12)].

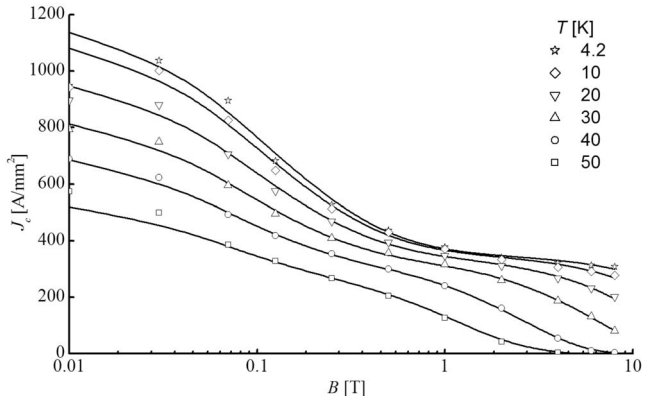

FIG. 20. Critical current density of Bi-2223 tape B-2 as a function of magnetic field at various temperatures, measured with a transport current. The magnetic field is applied perpendicular to the tape surface. The solid lines represent the critical current density according to classical flux-creep theory [Eq. (14)].

which interaction keeps the vortices at the grain boundaries in place. In YBCO, this mechanism is confirmed by several experimental studies.[70–74]

The coupling between AJ vortices at the grain boundaries and the strongly pinned vortices within the grains suggests that dissipation in the weakly linked network also occurs through flux creep. The magnetic field dependence of J_{cw} at 20 K is studied more closely in Fig. 19. Here J_{cw} is defined as the difference between J_c of a tape and J_c of the single-grained powder: $J_{cw}(B,T)=J_{c,\text{tape}}(B,T)-J_{c,\text{powder}}(B,T)$. A power-law dependence of J_{cw} versus magnetic field [Eq. (13)] fails to describe $J_{cw}(B)$, even when the value of parameter β is set equal to 2. The parameter β in Eq. (13) has to be increased to an even higher value to minimize the deviation. However, such a high value of β cannot be correlated with a physical mechanism. On the other hand, dissipation within the weakly linked network can be described accurately by Eq. (12), indicating that intergranular flux motion can be described with classical flux creep.

D. Modeling the overall J_c in Bi-2223 tapes

In the previous sections it became clear that dissipation in both the weakly linked network and the strongly linked backbone in Bi-2223 tapes can be well described with classical flux-creep theory. The overall J_c of a Bi-2223 tape is a summation of two contributions (J_{cw} and J_{cs}) that can both be described by Eq. (12) with a separate set of parameters $J_{c0,\ n}$ and B_{irr}. The overall J_c can thus be described as

$$J_c(B,T) = \frac{A_w}{A}J_{cw}(B,T) + \frac{A_s}{A}J_{cs}(B,T)$$
$$= \frac{A_w}{A}J_{cw}(0,T)\exp\left[-\left(\frac{B}{B_{\text{irr},w}(T)}\right)^{n_w}\ln\left(\frac{E_0(B)}{E_c}\right)\right]$$
$$+ \frac{A_s}{A}J_{cs}(0,T)\exp\left[-\left(\frac{B}{B_{\text{irr},s}(T)}\right)^{n_s}\ln\left(\frac{E_0(B)}{E_c}\right)\right]. \quad (14)$$

An example, where the overall J_c of a Bi-2223 tape is described by Eq. (14) is shown in Fig. 20. The magnetic field is applied perpendicular to the tape surface, and J_c is measured with a transport current. The solid lines are the parallel path model [Eq. (14)], where the parameter values are listed in Table I. The model describes $J_c(B,T)$ well over the entire magnetic field range, except for the lowest magnetic fields at low temperatures, where the self-field of the tape is comparable to the applied magnetic field. The self-field depends on the current running through the tape and is roughly 20–30 mT for a current of 100 A. The temperature dependence of $J_{cw}(0,T)$ and $J_{cs}(0,T)$ in Eq. (14) is plotted in Fig. 21(a). The critical current density at zero magnetic field of the strongly linked backbone is nearly independent of temperature below 40 K, while $J_{cw}(0,T)$ is dependent on temperature over the entire temperature range. Although $J_{cs}(0,T)$ is lower than $J_{cw}(0,T)$ at low temperatures, they become comparable for temperatures above 40 K. This general behavior is observed in a number of different Bi-2223 tapes (not shown here). The temperature dependences of the scaling fields $B_{\text{irr},w}(T)$ for the weakly linked network and $B_{\text{irr},s}(T)$ for the strongly linked backbone are shown in Fig. 21(b). The difference in pinning strength between both types of current paths follows directly from this comparison. Although this route is not followed in this paper, the accuracy with which parameters J_{cw} and J_{cs} in Eq. (14) are obtained can be increased by following the procedure to separate the contributions of both current paths directly from the experimental data, as described in Ref. 26.

The values of a number of parameters in Eq. (14) depend on the tape quality. For instance, a higher overall J_c will result in higher values of $J_{cw}(0,T)$ and $J_{cs}(0,T)$, due presumably to a larger cross section of both current paths. An enhancement in flux pinning will result in higher values of $B_{\text{irr},w}$ and $B_{\text{irr},s}$, although their dependence on temperature is expected to remain unchanged. The parameters that are listed in Table I (n_w, n_s, and E_0) are defined mainly by the intrinsic properties of the superconductor and do not change significantly between samples. This result has been confirmed by measuring the properties of a variety of Bi-2223 tapes, a result not presented in this paper.

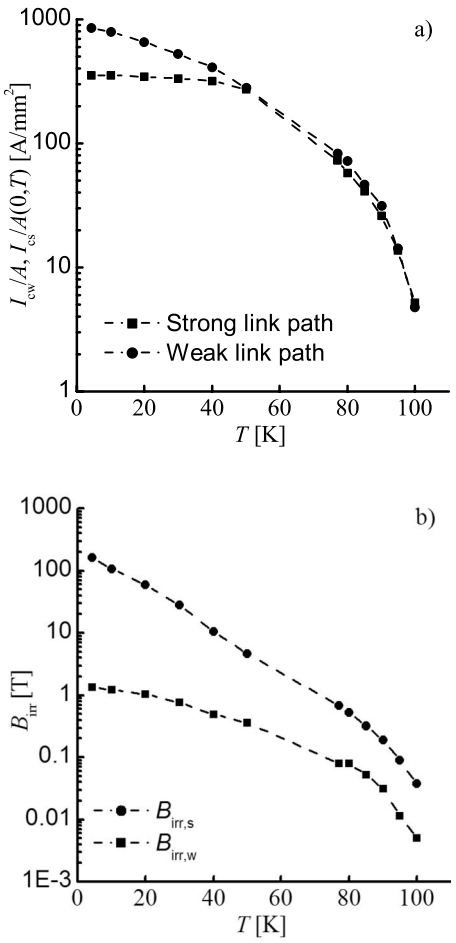

FIG. 21. (a) Temperature dependence of $I_{cw}(0,T)/A$ and $I_{cs}(0,T)/A$ of a Bi-2223 tape when I_c is measured with a transport current. (b) Temperature dependence of $B_{\mathrm{irr},w}(T)$ and $B_{\mathrm{irr},s}(T)$ when J_c is measured with a transport current.

V. CONCLUSIONS

The parallel path model is based on the assumption that two different types of current paths contribute to the overall critical current density in Bi-2223 tapes. The strongly linked backbone consists of grains that are connected at low angles, whereas the weakly linked network contains grains that are connected at slightly higher angles. Based on results that are reported in literature, the crossover occurs at an angle of about 4°. Grains that are connected at angles exceeding 8° form Josephson weak links and do not significantly contribute to the overall critical current density. Dissipation in the strongly linked backbone occurs mainly at high magnetic fields and is situated within the grains through intragranular flux creep. Dissipation in the weakly linked network occurs at grain boundaries through intergranular flux creep. In both current paths, flux motion can be described through classical flux-creep theory.

Several experiments were presented that support the parallel path model. The contributions of both current paths were studied separately by grinding a Bi-2223 tape into a single-grained powder. This method destroys the weakly linked network in the Bi-2223 core of the tape by breaking up the grain boundaries. Dissipation in the powder occurs entirely through intragranular flux motion, as was confirmed by comparing dissipation in both tape and powder. The powder shows a strongly reduced critical current density at low and intermediate magnetic fields compared to that of the tape. No significant change in dissipation was measured at high magnetic field.

By analyzing the magnetic field dependence of the overall critical current density as a function of axial strain, it was found that the critical current density at low magnetic fields (where the weakly linked current path has a significant contribution) is more sensitive to axial strain than that at high magnetic fields (where only the strongly linked backbone carries current). Scanning-electron micrographs showed that microcracks develop mainly at grain boundaries when strain exceeds the irreversible strain limit. This confirms that grains that are connected at low angle are mechanically stronger than grains that are connected at angles larger than 4°.

The dependence of the critical current density of Bi-2223 tapes on magnetic field that is applied parallel to the tape surface is described in terms of its dependence on magnetic field applied perpendicular to the tape surface over a wide temperature range of 15–77 K. Such an accurate description is possible only when the contributions of the weakly linked network and the strongly linked backbone are separately considered. Differences in dissipation mechanism in both current paths are revealed by a difference in sensitivity to magnetic field applied parallel to the tape surface. For instance, the critical current density of the strongly linked backbone becomes more isotropic in terms of magnetic field direction when the tape is cooled below 50 K, while such behavior is not measured for the critical current density of the weakly linked network.

ACKNOWLEDGMENTS

This work was supported by the (U.S.) Air Force Office of Scientific Research, by the National Science Foundation under Contract No. DMR-9527035, by the (U.S.) Department of Energy, Office of Electricity Delivery and Energy Reliability, and FOM (Fundamental Research on Matter), which is financially supported by NWO (the Dutch Organization for Scientific Research).

[1] C. S. Weber, R. Lee, S. Ringo, T. Masuda, H. Yumura, and J. Moscovic, IEEE Trans. Appl. Supercond. **17**, 2038 (2007).

[2] J. A. Demko, I. Sauers, D. R. James, M. J. Gouge, D. Lindsay, M. Roden, J. Tolbert, D. Willén, and C. Træholt, IEEE Trans. Appl. Supercond. **17**, 2047 (2007).

[3] S. S. Kalsi, D. Madura, and M. Ingram, IEEE Trans. Appl. Supercond. **15**, 2146 (2005).

[4] V. Selvamanickam, Y. Chen, X. Xiong, Y. Y. Xie, J. L. Reeves, X.

Zhang, Y. Qiao, T. M. Salagaj, Y. Li, K. P. Lenseth, and R. M. Schmidt, IEEE Trans. Appl. Supercond. **17**, 3231 (2007).
[5] M. Kikuchi, T. Kato, K. Ohkura, N. Ayai, J. Fujikami, K. Fujino, S. Kobayashi, E. Ueno, K. Yamazaki *et al.*, Physica C **445-448**, 717 (2006).
[6] L. N. Bulaevskii, J. R. Clem, L. I. Glazman, and A. P. Malozemoff, Phys. Rev. B **45**, 2545 (1992).
[7] L. N. Bulaevskii, L. L. Daemen, M. P. Maley, and J. Y. Coulter, Phys. Rev. B **48**, 13798 (1993).
[8] B. Hensel, J.-C. Grivel, A. Jeremie, A. Perin, A. Pollini, and R. Flükiger, Physica C **205**, 329 (1993).
[9] B. Hensel, G. Grasso, and R. Flükiger, Phys. Rev. B **51**, 15456 (1995).
[10] D. C. Larbalestier, A. Gurevich, D. M. Feldmann, and A. A. Polyanskii, Nature (London) **414**, 368 (2001).
[11] R. Kleiner, F. Steinmeyer, G. Kunkel, and P. Müller, Phys. Rev. Lett. **68**, 2394 (1992).
[12] R. Kleiner and P. Müller, Phys. Rev. B **49**, 1327 (1994).
[13] J. H. Cho, M. P. Maley, J. O. Willis, J. Y. Coulter, L. N. Bulaevskii, P. Halder, and L. R. Motowidlo, Appl. Phys. Lett. **64**, 3030 (1994).
[14] D. Dimos, P. Chaudhari, J. Mannhart, and F. K. Legoues, Phys. Rev. Lett. **61**, 219 (1988).
[15] D. Dimos, P. Chaudhari, and J. Mannhart, Phys. Rev. B **41**, 4038 (1990).
[16] N. F. Heinig, R. D. Redwing, I. Fei Tsu, A. Gurevich, J. E. Nordman. S. E. Babcock, and D. C. Larbalestier, Appl. Phys. Lett. **69**, 577 (1996).
[17] T. Amrein, L. Schultz, B. Kabius, and K. Urban, Phys. Rev. B **51**, 6792 (1995).
[18] J. Hänisch, A. Attenberger, B. Holzapfel, and L. Schultz, Phys. Rev. B **65**, 052507 (2002).
[19] A. Attenberger, J. Hänisch, B. Holzapfel, and L. Schultz, Physica C **372-376**, 649 (2002).
[20] M. Dhallé, M. Cuthbert, M. D. Johnston, J. Everett, R. Flükiger, S. X. Dou, W. Goldacker, T. Beales, and A. D. Caplin, Supercond. Sci. Technol. **10**, 21 (1997).
[21] Y. K. Huang, B. ten Kate, and H. H. J. ten Kate, Physica C **309**, 197 (1998).
[22] D. C. van der Laan, H. J. N. van Eck, B. ten Haken, J. Schwartz, and H. H. J. ten Kate, IEEE Trans. Appl. Supercond. **11**, 3345 (2001).
[23] D. C. van der Laan, H. J. N. van Eck, J. Schwartz, B. ten Haken, and H. H. J. ten Kate, Physica C **372-376**, 1024 (2002).
[24] J. W. Ekin, T. M. Larson, A. M. Hermann, Z. Z. Sheng, K. Togano, and H. Kumakura, Physica C **160**, 489 (1989).
[25] Y. Yeshurun, A. P. Malozemoff, and A. Shaulov, Rev. Mod. Phys. **68**, 911 (1996).
[26] J. Horvat, S. X. Dou, H. K. Liu, and R. Bhasale, Physica C **271**, 51 (1996).
[27] E. J. Kramer, J. Appl. Phys. **44**, 1360 (1973).
[28] C. P. Bean, Phys. Rev. Lett. **8**, 250 (1962).
[29] R. Wesche, Physica C **246**, 186 (1995).
[30] J. E. Tkaczyk, R. H. Arendt, M. F. Garbauskas, H. R. Hart, K. W. Lay, and F. E. Luborsky, Phys. Rev. B **45**, 12506 (1992).
[31] M. N. Cuthbert, M. Dhallé, J. Thomas, A. D. Caplin, S. X. Dou, Y. C. Guo, H. K. Lin, R. Flükiger, G. Grasso, W. Goldacker, and J. Kessler, IEEE Trans. Appl. Supercond. **5**, 1391 (1995).
[32] M. Dhallé, F. Marti, G. Grasso, A. Perin, J. C. Grivel, E. Walker, and R. Flükiger, Physica C **282-287**, 1173 (1997).
[33] P. H. Kes, J. Aarts, V. M. Vinokur, and C. J. van der Beek, Phys. Rev. Lett. **64**, 1063 (1990).
[34] M. Dhallé, D. C. van der Laan, H. J. N. van Eck, L. Vargas, B. ten Haken, H. H. J. ten Kate, U. P. Trociewitz, and J. Schwartz, IEEE Trans. Appl. Supercond. **13**, 3702 (2003).
[35] J. W. Ekin, D. K. Finnemore, Qiang Li, J. ten Brink, and W. Carter, Appl. Phys. Lett. **61**, 858 (1992).
[36] R. Passerini, M. Dhallé, E. Giannini, G. Witz, B. Seeber, and R. Flükiger, Physica C **371**, 173 (2002).
[37] H. Kitaguchi, K. Itoh, H. Kumakura, T. Takeuchi, K. Togano, and H. Wada, IEEE Trans. Appl. Supercond. **11**, 3058 (2001).
[38] B. ten Haken, A. Beuink, and H. H. J. ten Kate, IEEE Trans. Appl. Supercond. **7**, 2034 (1997).
[39] M. Polak, J. A. Parrell, A. A. Polyanskii, A. E. Pashitski, and D. C. Larbalestier, Appl. Phys. Lett. **70**, 1034 (1997).
[40] M. R. Koblischka, T. H. Johansen, and H. Bratsberg, Supercond. Sci. Technol. **10**, 693 (1997).
[41] D. C. van der Laan, H. J. N. van Eck, B. ten Haken, H. H. J. ten Kate, and J. Schwartz, IEEE Trans. Appl. Supercond. **13**, 3534 (2003).
[42] M. T. Malachevsky and C. A. D'Ovidio, Supercond. Sci. Technol. **18**, 289 (2005).
[43] R. Passerini, M. Dhallé, B. Seeber, and R. Flükiger, Supercond. Sci. Technol. **15**, 1507 (2002).
[44] D. C. van der Laan, J. W. Ekin, H. J. N. van Eck, M. Dhallé, B. ten Haken, M. W. Davidson, and J. Schwartz, Appl. Phys. Lett. **88**, 022511 (2006).
[45] J. L. Wang, X. Y. Cai, R. J. Kelley, M. D. Vaudin, S. E. Babcock, and D. C. Larbalestier, Physica C **230**, 1898 (1994).
[46] M. Tachiki and S. Takahashi, Solid State Commun. **70**, 291 (1989).
[47] M. Tachiki and S. Takahashi, Solid State Commun. **72**, 1083 (1989).
[48] G. Blatter, M. V. Feigel'man, V. B. Geshkenbein, A. I. Larkin, and V. M. Vinokur, Rev. Mod. Phys. **66**, 1125 (1994).
[49] V. Hussennether, O. Waldmann, P. Müller, M. Leghissa, and H.-W. Neumüller, Phys. Rev. B **62**, 9808 (2000).
[50] R. Flükiger, B. Hensel, A. Jeremie, M. Decroux, H. Küpfer, W. Jahn, W. Goldacker, Y. Yamada, and J. Q. Xu, Supercond. Sci. Technol. **5**, S61 (1992).
[51] Q. Y. Hu, H. W. Weber, H. K. Liu, S. X. Dou, and H. W. Nuemüller, Physica C **252**, 211 (1995).
[52] M. P. Maley, P. J. Kung, J. Y. Coulter, W. L. Carter, G. N. Riley, and M. E. McHenry, Phys. Rev. B **45**, 7566 (1992).
[53] B. Lehndorff, M. Hortig, and H. Piel, Supercond. Sci. Technol. **11**, 1261 (1998).
[54] O. van der Meer, B. ten Haken, and H. H. J. ten Kate, Physica C **357-360**, 1174 (2001).
[55] P. W. Anderson, Phys. Rev. Lett. **9**, 309 (1962).
[56] E. Zeldov, N. M. Amer, G. Koren, A. Gupta, R. J. Gambino, and M. W. McElfresh, Phys. Rev. Lett. **62**, 3093 (1989).
[57] E. Zeldov, N. M. Amer, G. Koren, A. Gupta, M. W. McElfresh, and R. J. Gambino, Appl. Phys. Lett. **56**, 680 (1990).
[58] M. P. Maley, J. O. Willis, H. Lessure, and M. E. McHenry, Phys. Rev. B **42**, 2639 (1990).
[59] G. Fuchs, E. S. Vlakhov, K. A. Nenkov, T. Staiger, and A. Gladun, Physica C **247**, 340 (1995).
[60] A. A. Polyanskii, A. Gurevich, A. E. Pashitski, N. F. Heinig, R. D. Redwing, J. E. Nordman, and D. C. Larbalestier, Phys. Rev. B **53**, 8687 (1996).

[61] H. Küpfer, I. Apfelstedt, R. Flükiger, C. Keller, R. Meier-Hirmer, B. Runtsch, A. Turowski, U. Wiech, and T. Wolf, Cryogenics **28**, 650 (1988).
[62] T. Wolf and A. Majhofer, Phys. Rev. B **47**, 5383 (1993).
[63] P. Muné and J. López, Physica C **257**, 360 (1996).
[64] K.-H. Müller and A. J. Pauza, Physica C **161**, 319 (1989).
[65] K.-H. Müller, D. N. Matthews, and R. Driver, Physica C **191**, 339 (1992).
[66] R. L. Peterson and J. W. Ekin, Physica C **157**, 325 (1989).
[67] A. Gurevich and L. D. Cooley, Phys. Rev. B **50**, 13563 (1994).
[68] X. Y. Cai, A. Gurevich, I. Fei Tsu, D. L. Kaiser, S. E. Babcock, and D. C. Larbalestier, Phys. Rev. B **57**, 10951 (1998).
[69] A. Gurevich and L. D. Cooley, Phys. Rev. B **50**, 13563 (1994).
[70] D. Kim, P. Berghuis, M. B. Field, D. J. Miller, K. E. Gray, R. Feenstra, and D. K. Christen, Phys. Rev. B **62**, 12505 (2000).
[71] J. Albrecht, S. Leonhardt, and H. Kronmüller, Phys. Rev. B **63**, 014507 (2000).
[72] K. E. Gray, D. J. Miller, M. B. Field, D. H. Kim, and P. Berghuis, Physica C **341-348**, 1397 (2000).
[73] P. Berghuis, D. J. Miller, D. H. Kim, K. E. Gray, R. Feenstra, and D. K. Christen, IEEE Trans. Appl. Supercond. **11**, 3868 (2001).
[74] A. Gurevich, M. S. Rzchowski, G. Daniels, S. Patnaik, B. M. Hinaus, F. Carillo, F. Tafuri, and D. C. Larbalestier, Phys. Rev. Lett. **88**, 097001 (2002).